Inflammation, Vol. 42, No. 3, June 2019 (© 2018)
DOI: 10.1007/s10753-018-0940-2

ORIGINAL ARTICLE

Peroxisome Proliferator-Activated Receptor γ Agonist Rosiglitazone Protects Blood–Brain Barrier Integrity Following Diffuse Axonal Injury by Decreasing the Levels of Inflammatory Mediators Through a Caveolin-1-Dependent Pathway

Yonglin Zhao,[1] Xing Wei,[2] Jinning Song,[3] Ming Zhang,[4] Tingqin Huang,[4] and Jie Qin[5,6]

Abstract—Our early experiments confirmed that rosiglitazone (RSG), a peroxisome proliferator-activated receptor γ (PPARγ) agonist, had therapeutic potential for the treatment of diffuse axonal injury (DAI) by inhibiting the expression of amyloid-beta precursor protein and reducing the loss and abnormal phosphorylation of tau, but the underlying mechanisms were not fully defined. In this study, we aimed to investigate a possible role for PPARγ in the protection of blood–brain barrier (BBB) integrity in a rat model of DAI, and the underlying mechanisms. PPAR agonists and antagonists were intraperitoneally injected after DAI. Treatment with RSG ameliorated axonal injury, cell apoptosis, glia activation, and the release of inflammatory factors such as TNF-α, IL-1β, and IL-6. It also increased the expression of tight junction-associated proteins like ZO-1, claudin-5, and occludin-1, whereas the PPARγ antagonist GW9662 had the opposite effects. These effects were also studied in a BBB *in vitro* model, consisting of a monolayer of human microvascular endothelial cells (HBMECs) subjected to oxygen and glucose deprivation (OGD). Treatment with RSG ameliorated the loss of BBB integrity and the increased permeability induced by OGD by reducing the release of inflammatory factors and maintaining the expression of tight junction-associated proteins. Interestingly, caveolin-1 was found located mainly in endothelial cells, and RSG increased the expression of caveolin-1, which decreased following OGD. In contrast, caveolin-1 siRNA abrogated the protective effects of RSG in the *in vitro* BBB model. In conclusion, we provide evidence that PPARγ plays an important role in a series of processes associated with DAI, and

[1] Department of Oncology, the Second Affiliated Hospital of Xi'an Jiaotong University, Xi'an, 710004, China
[2] Department of Gynaecology and Obstetrics, the Second Affiliated Hospital of Xi'an Jiaotong University, Xi'an, 710004, China
[3] Department of Neurosurgery, the First Affiliated Hospital of Xi'an Jiaotong University, Xi'an, 710061, China
[4] Department of Neurosurgery, the Second Affiliated Hospital of Xi'an Jiaotong University, Xi'an, 710004, China
[5] Department of Orthopedics, the Second Affiliated Hospital of Xi'an Jiaotong University, No. 157 Xiwu Road, Xi'an, 710004, People's Republic of China
[6] To whom correspondence should be addressed at Department of Orthopedics, the Second Affiliated Hospital of Xi'an Jiaotong University, No. 157 Xiwu Road, Xi'an, 710004, People's Republic of China. E-mail: icyhawk@163.com

that the PPARγ agonist RSG can protect BBB integrity by decreasing the levels of inflammatory mediators through a caveolin-1-dependent pathway.

KEY WORDS: Peroxisome proliferator-activated receptor γ; Caveolin-1; Blood–brain barrier; Diffuse axonal injury.

INTRODUCTION

Diffuse axonal injury (DAI) is a prominent feature of human traumatic brain injury (TBI) and a major cause of subsequent morbidity. Although some advances have been made in the treatment of DAI, the pathogenesis of DAI remains unclear and there is still no effective treatment for axonal disconnection. The blood–brain barrier (BBB), which plays a key role in normal brain physiological regulation, is composed in part of endothelial cells connected by tight junction proteins, astrocyte podocytes, a basement membrane, and pericytes. Dysfunction of any one of these cell types can jeopardize BBB integrity [1]. The tight junction-associated proteins include zonula occludens-1 (ZO-1), claudins, and occludin. The signaling pathways related to tight junction regulation include G-proteins, serine-, threonine- and tyrosine-kinases, and extra and intracellular calcium levels. Several cytokines, such as interleukin 1β (IL-1β), interleukin 6 (IL-6), and tumor necrosis factor-α (TNF-α), also play important regulatory roles [2, 3].

Rosiglitazone (RSG), a peroxisome proliferator-activated receptor γ (PPARγ) agonist, has been shown to exert a neuroprotective effect in many nervous system pathologic conditions, such as traumatic brain injury, focal cerebral ischemia, and intracerebral hemorrhage [4, 5]. For example, RSG has shown anti-inflammatory and neuroprotective effects in rat models of traumatic injury and spinal cord injury. Our previous study also showed that RSG could have therapeutic potential in DAI by inhibiting the expression of amyloid-beta precursor protein and reducing the loss and abnormal phosphorylation of tau [6]. However, the underlying mechanisms remain elusive.

PPAR agonists have been shown to stabilize BBB permeability and improve the neurological outcome in PPAR-dependent as well as independent manners [8]. Caveolin-1, identified as the principal marker of caveolae in endothelial cells, plays an important role in several physiological and pathological BBB processes [7]. Interestingly, RSG was shown to dose and time-dependently increase caveolin-1 expression by activating PPARγ [9]. However, it is still unknown whether this PPARγ agonist can protect against DAI by stabilizing the BBB and whether it modifies the levels of inflammatory mediators. It is also unknown whether caveolin-1 plays any role in PPARγ-mediated effects.

In the present study, we investigated the role played by PPARγ in axonal injury, cell apoptosis, glia activation, BBB integrity, and the release of inflammatory factors. We also explored the localization of caveolin-1 and assessed the effects of PPARγ activation on the expression of caveolin-1 and tight junction-associated proteins. Finally, an *in vitro* model of BBB dysfunction was established by subjecting human microvascular endothelial cell (HBMEC) monolayers to oxygen deprivation (OGD). Expression of caveolin-1 was directly and specifically down-regulated in these monolayer cultures by transduction with an adenoviral construct encoding caveolin-1 small interfering RNA (siRNA). BBB integrity and the levels of inflammatory factors were monitored. Our results showed that PPARγ played an important role in a series of processes that lead to injury and destruction of the BBB following DAI. Specifically, the PPARγ agonist RSG protected BBB integrity by decreasing the level of inflammatory factors through a caveolin-1-dependent pathway.

MATERIALS AND METHODS

Ethics

All procedures were performed according to the Guidelines and Suggestions for the Care and Use of Laboratory Animals formulated by the Ministry of Science and Technology of the People's Republic of China (PRC) and the Guidelines for the Care and Use of Laboratory Animals from the National Institutes of Health (NIH Publication no. 80-23). The Biomedical Ethics Committee for Animal Experiments of Shaanxi Province (China) approved this study. Animals were anesthetized with sodium pentobarbital, and all efforts were made to minimize suffering.

Animals and Groups

Male adult Sprague–Dawley (SD) rats (weighing 250–300 g, 8–10 weeks old) were provided by the Experimental Animal Center of Xi'an Jiaotong University [license no. SCXK (Shaanxi) 2006-001]. Rats were maintained in groups of four per cage, at an ambient temperature

of 22 ± 1 °C, with a 12-h light/dark cycle, and with an unlimited supply of food and water. A total of 96 SD rats were divided into the following four groups: control group (24 rats), DAI 1 d group (24 rats), DAI 1 d + RSG group (24 rats), and DAI 1 d + GW9662 group (24 rats). Each test was performed independently three times per rat. RSG (Cayman Chemical Co., Ann Arbor, MI, USA) was diluted with saline to a final concentration of 2 mg/mL prior to injection and was intraperitoneally injected immediately after DAI at a dose of 10 mg/kg, followed by repeated injections every 12 h. GW9662 (Cayman Chemical Co., Ann Arbor, MI, USA) was dissolved in dimethyl sulfoxide (DMSO), diluted with saline, and intraperitoneally injected (4 mg/kg) immediately after DAI, followed by repeated injections every 12 h.

Animal Model of DAI

A lateral head rotation device was used to establish the DAI model, as in our previous studies [10]. Briefly, after intraperitoneally injecting the rat with 1% (*w*/*v*) pentobarbital sodium (35 mg/kg), its head was horizontally secured to the device by two pins anchoring the ears and by an anterior tooth hole, with its body at an oblique angle of 30° with respect to the top of the laboratory table. Once the trigger was pushed, the rat's head was rotated by 90°, subjecting it to sudden acceleration and deceleration. Rats in the control group were only anesthetized and fixed to the device but did not suffer injury. Rats in the DAI groups became comatose and regained consciousness about half an hour later. The vital signs of comatose rats were monitored to prevent suffocation. For the following approximately 12 h, a weakened response to stimulation, unstable gait, and reduced activity and food intake were observed in all injured rats. Next, rats were euthanized with an intraperitoneal injection of 5% (*w*/*v*) pentobarbital sodium (150 mg/kg), perfused with normal saline, and then with 4% (*w*/*v*) buffered paraformaldehyde, pH 7.4. The brains were removed, post-fixed, embedded in paraffin, and cut into sections. Three rats died after injury and were replaced with new rats.

Cell Culture and Treatment

Human brain microvascular endothelial cells (HBMEC, ScienCell Research Laboratories, San Diego, CA, USA) were grown as a monolayer in culture medium containing 10% fetal bovine serum (FBS; Sigma, St. Louis, MO, USA), at 37 °C in a humidified atmosphere with 5% CO_2 and 95% air. HBMEC were seeded onto collagen-coated transwells for 4 days, until the transendothelial electric resistance (TEER) reached > 250 μΩ/cm^2. RSG was dissolved in culture medium at a final concentration of 50 μmol/L. This concentration was selected based on previous studies [11, 12].

Small Interfering RNA (siRNA) Transfection

In vitro transfection was performed according to the method described in previous studies [13, 14]. Briefly, HBMECs at 70–80% confluence were transfected with 100 pmol of siRNA (sc-29241, Santa Cruz Biotech, Santa Cruz, CA, USA) or negative-control siRNA (sc-36869, Santa Cruz Biotech, Santa Cruz, CA, USA) using lipofectamine 2000 (Life Technologies, Carlsbad, CA, USA), according to the manufacturer's instructions and previous studies [15, 16]. After 6 h, the culture was replaced with fresh medium and cells were grown for another 24 h. Specific silencing was confirmed by Western blot. Twenty-four hours after transfection, cells were subjected to OGD and treated with RSG.

Oxygen-Glucose Deprivation (OGD)

Cells were divided into the following four groups: control group, OGD group, OGD + RSG group, and OGD + cav-1 siRNA+RSG group. In the control group, HBMECs were not exposed to OGD. In the OGD groups, growth media were replaced with 10% FBS DME media without glucose. Then, cell culture preparations were placed in an anaerobic chamber that was filled with 5% CO_2 and 95% N_2 (*v*/*v*), and the chamber was moved to a 37 °C incubator. RSG was added 30 min before OGD [17, 18]. After 6 h of OGD, conditioned media were collected and stored at − 80 °C for subsequent immunoassays, while the cells were harvested, centrifuged, and the pellets were stored for Western blot analysis.

Transendothelial Electrical Resistance (TEER) Measurement

Cells were seeded onto Transwell inserts (pore size 0.4 μm, effective growth area 0.3 cm^2, BD Bioscience, Sparks, MD, USA) and grown for 4 days. The TEER was measured with a millicell-ERS instrument (Millipore, Billerica, MA, USA). The resistance of blank filters was subtracted from that of cell-coated filters before the final resistance values were calculated [19]. The final TEER values were measured in μΩ/cm^2.

Horseradish Peroxidase (HRP) Flux

To measure the permeability of the *in vitro* BBB model, HRP flux experiments were performed. Briefly, serum-free culture media containing 0.5 μM HRP (Sigma-Aldrich, St. Louis, MO, USA) were added to the upper compartment of the transwells. One hour later, the culture medium in the lower compartment was collected and the amount of HRP was quantified as described previously [20, 21]. The HRP flux was expressed in nanograms per milliliter.

Transmission Electron Microscopy (TEM)

TEM was performed as described in our previous study [10]. Briefly, cortices were cut, trimmed, and post-fixed at 4 °C. Samples were fixed in 1% (*w*/*v*) osmium tetroxide for 2 h at 4 °C. Subsequently, sample blocks were dehydrated by immersing them in a series of ethanol solutions of increasing concentration, followed by resin embedding in Epon 812, and cutting the samples into 1–2 μm sections. After methylene blue staining, semithin sections were cut into thin sections (50–70 nm) using an ultrathin microtome. Then, thin sections were lightly counterstained with 2% (*w*/*v*) uranyl acetate and 3% (w/v) lead citrate prior to examination with a TEM (H-7650, Hitachi, Tokyo, Japan).

Hematoxylin and Eosin (H&E) Staining and Golgi Silver Staining

Sections were stained with hematoxylin and eosin or processed for Golgi staining with the FD Rapid GolgiStain™ Kit (FD NeuroTechnologies, Inc., Columbia, MD, USA), according to the manufacturer's instructions. Three sections per animal were processed for H&E staining and Silver Staining. Stained sections were examined with a light microscope (BX-40, Olympus, Tokyo, Japan) at × 40 magnification.

Immumohistochemical Staining

Immunohistochemical staining was performed as previously described [10]. Tissue sections were incubated overnight at 4 °C with mouse monoclonal tau46 antibody (4019, 1:300, Cell Signaling Technology, Danvers, MA, USA), rabbit monoclonal anti-neurofilament light chain (2837, NF-L, 1:100, Cell Signaling Technology, Danvers, MA, USA), mouse monoclonal anti-neurofilament heavy chain (2836, NF-H, 1:100, Cell Signaling Technology, Danvers, MA, USA), or mouse monoclonal anti-neurofilament medium chain (2838, NF-M, 1:100, Cell Signaling Technology, Danvers, MA, USA). Sections were incubated for 1 h with HRP-conjugated secondary antibodies (1:500) and, after adding diaminobenzidine, examined under the microscope. Immunohistochemical scores (IHS) were calculated based on the percentage of positive cells and the staining intensity by means of Image-Pro Plus 6.0 software (Media Cybernetics, Rockville, MD, USA). (1) The percentage of positive cells was rated on a scale from 0 to 4, defined as follows: no staining, 0; 1–10% of cells stained, 1; 11–50%, 2; 51–80%, 3; and 81–100%, 4. (2) The staining intensity was rated on a scale from 0 to 3, as follows: 0 = negative, 1 = weak, 2 = moderate, and 3 = strong. Theoretically, the scores could range from 0 to 12. An IHS of 9–12 was considered strong immunoreactivity, 5–8 was considered moderate, 1–4 was considered weak, and 0 was considered negative [22].

Immunofluorescence Staining

Sections were deparaffinized and rehydrated before inactivating endogenous peroxidases with 3% (*v*/*v*) H_2O_2. Sections were then blocked with serum after antigen unmasking and incubated with the following primary antibodies: rabbit monoclonal anti-caveolin-1 (3267, 1: 400, Cell Signaling Technology, Danvers, MA, USA), mouse monoclonal anti-NeuN (1:400, Millipore, Billerica, MA, USA), mouse monoclonal anti-GFAP, goat polyclonal anti-Iba-1 (1:200, Abcam, Cambridge, UK), or anti-CD34 antibody (ICO115, 1:200, Novus Biological, Littleton, Colorado, USA). After overnight incubation at 4 °C, secondary fluorescent antibodies were added for 1 h at 37 °C, and the nuclei were stained with 4′,6-diamidino-2-phenylindole (DAPI, 1 μg/ml) for 10 min. The sections were observed using a fluorescence microscope (Molecular Devices, Sunnyvale, CA, USA).

Terminal Deoxynucleotidyl Transferase-Mediated Digoxigenin-DUTP-Biotin Nick-End Labeling (TUNEL) Assay

Apoptosis in the rat cortex was detected with the DeadEnd™ Fluorometric TUNEL System (Promega, Madison, Wisconsin, USA), following the manufacturer's instructions. Briefly, the sections were immersed in 0.2% (*v*/*v*) Triton® X-100/PBS for 5 min, incubated in equilibration buffer, and equilibrated at room temperature, followed by the TdT reaction at 37 °C. The nuclei were stained with DAPI. The number of TUNEL positive cells

was counted in six nonadjacent random fields by fluorescence microscopy.

Western Blot

Brain tissue was removed and stored in liquid nitrogen. Tissue was later thawed, homogenized, and total proteins were extracted using a total protein extraction reagent kit. Equal amounts of protein samples were loaded onto SDS-PAGE gels, electrophoretically separated and transferred to immobilon-P/PVDF membranes (Millipore Corp, Billerica, MA, USA), followed by blocking with 5% skim milk (diluted in TBST) at 37 °C for 1 h. Membranes were then incubated overnight at 4 °C with the following antibodies: rabbit monoclonal anti-caveolin-1 (3267, 1:1000, Cell Signaling Technology, Danvers, MA, USA), goat polyclonal anti-ZO-1 (ab190085, 1:1000, Abcam, Cambridge, UK), rabbit monoclonal anti-claudin-5 (ab131259, 1:1000, Abcam, Cambridge, UK), rabbit monoclonal anti-β-actin antibody (1:1000, Cell Signaling Technology, Danvers, MA, USA), or rabbit monoclonal anti-occludin-1 (ab167161, 1:1000, Abcam, Cambridge, UK). Next, membranes were incubated with the corresponding secondary antibodies at 37 °C for 1 h. Enhanced chemiluminescence signals were visualized using the ChemiDoc MP System (Bio-Rad protein assay, Bio-Rad, Segrate, Italy). Densitometric quantification of the bands was performed using the Image J software (version 1.29x: NIH, Bethesda, MD, USA). Values obtained were normalized based on the density values of β-actin as an internal control.

Enzyme-Linked Immunosorbent Assay (ELISA)

IL-1β, IL-6, and TNF-α assay kits (R&D Systems, Minneapolis, MN, USA) were used to measure the levels of proinflammatory cytokines as previously described [10]. Tissue cytokine concentrations were expressed as picograms per milligram of protein.

BBB Permeability Assay

The permeability of the BBB was determined by measuring the penetration of Evans blue (Sigma-Aldrich, St. Louis, MO, USA) into the brain tissue. Evans blue was dissolved in saline at 2% (*w*/*v*) and was intravenously administered (4 mL/kg of body weight) *via* the tail vein 1 h before measurement. Each brain was then quickly removed, weighed, and homogenized and proteins were precipitated with 50% trichloroacetic acid overnight. After centrifuging for 30 min, the absorbance at a wavelength of 610 nm was measured in the supernatant. The extravasation of Evans blue was expressed as microgram per gram brain tissue.

Evaluation of Brain Edema

The standard wet-dry method was used to evaluate the brain water content (BWC). The brains were quickly removed and their wet weight was measured. Brains were then dried in an oven at 105 °C for 72 h and their dry weight was determined. BWC was calculated by the formula BWC = [(wet weight − dry weight) / wet weight].

Statistical Analysis

Data are presented as the mean ± SD and statistical analyses were performed with SPSS 18.0 (SPSS, Chicago, IL, USA). Numerical data from more than two groups were analyzed by one-way ANOVA, followed by an LSD (L) *post hoc* test. A P value < 0.05 was considered statistically significant.

RESULTS

Pathological Changes in the DAI Rat Model

Histopathological features were examined to evaluate the validity of the DAI model by H&E staining, silver staining, and TEM. H&E staining revealed neuronal pyknosis, swelling, torsion, and cell body deformation in the cortices of rats from the DAI 1 d group. In contrast, no abnormalities were observed in the control group (Fig. 1). Silver staining revealed smooth, continuous axons in the control group. In contrast, many axons were fractured and showed discontinuous structures in the DAI group. TEM examination of longitudinal sections of axons was conducted to demonstrate ultrastructural alterations. In the control group, consecutive, integral, and compact microtubules were observed. In contrast, in the DAI 1 d group, the microtubules were disordered, discontinuous, frayed, and displayed conspicuous free ends (Fig. 1).

Role of PPARγ in Axonal Injury, Glia Response, and Cell Apoptosis After DAI

To investigate the role played by PPARγ in axonal injury and the glia response after DAI, the expression of NF-L, NF-M, NF-H, tau, GFAP, and Iba-1 was assessed by immunostaining in rat cortices. NF-L, NF-M, and NF-H

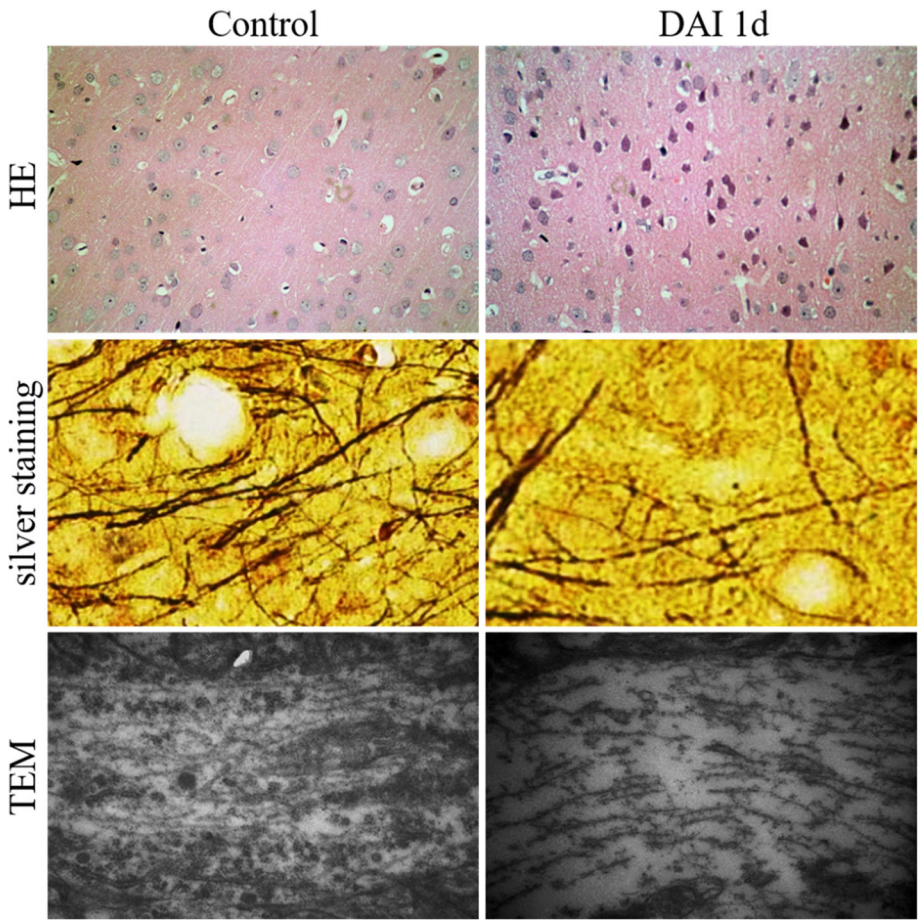

Fig. 1. Identification of pathological features in the rat cortex after DAI. Pathological changes in rat cortices in the DAI 1 d and control groups observed by H&E staining, silver stain (× 40 magnification, $n = 6$), and TEM (× 40,000 magnification).

were rarely detected in the control group. In contrast, the expression of NF-L, NF-M, and NF-H was increased in the DAI 1 d, DAI 1 d + RSG, and DAI 1 d + GW9662 groups. Importantly, when compared with the DAI 1 d group, RSG decreased the expression of NF-L, NF-M, and NF-H, whereas GW9662 significantly increased their expression. In addition, axons in the control group were tau-positive and the expression of tau decreased following DAI. When compared with the DAI 1 d group, RSG increased the expression of tau, while GW9662 significantly decreased its expression (Fig. 2).

When compared with the control group, the numbers of Iba-1-positive microglial cells, GFAP-positive astrocytes, and apoptotic cells were significantly increased in the cortex 1 d after DAI. RSG treatment significantly reduced the number of activated microglial cells, astrocytes, and apoptotic cells 1 d after DAI, whereas GW9662 increased GFAP and Iba-1 expression and increased the number of apoptotic cells (Figs. 3 and 4).

Role Played by PPARγ in the Regulation of the Permeability and Integrity of the BBB

To investigate a possible role of PPARγ in the regulation of the permeability and integrity of the BBB following DAI, we relied on Evans blue to monitor the destruction of the BBB, BWC to measure brain edema, and TEM ultrastructural examination. Our results showed that DAI induced significant brain edema, which was significantly inhibited by RSG treatment in the DAI 1 d + RSG group, whereas the PPARγ inhibitor GW9662 had the opposite effect: it exacerbated the edema. Indeed, very little Evans blue diffusion was detected in the control group, whereas the levels of Evans blue significantly

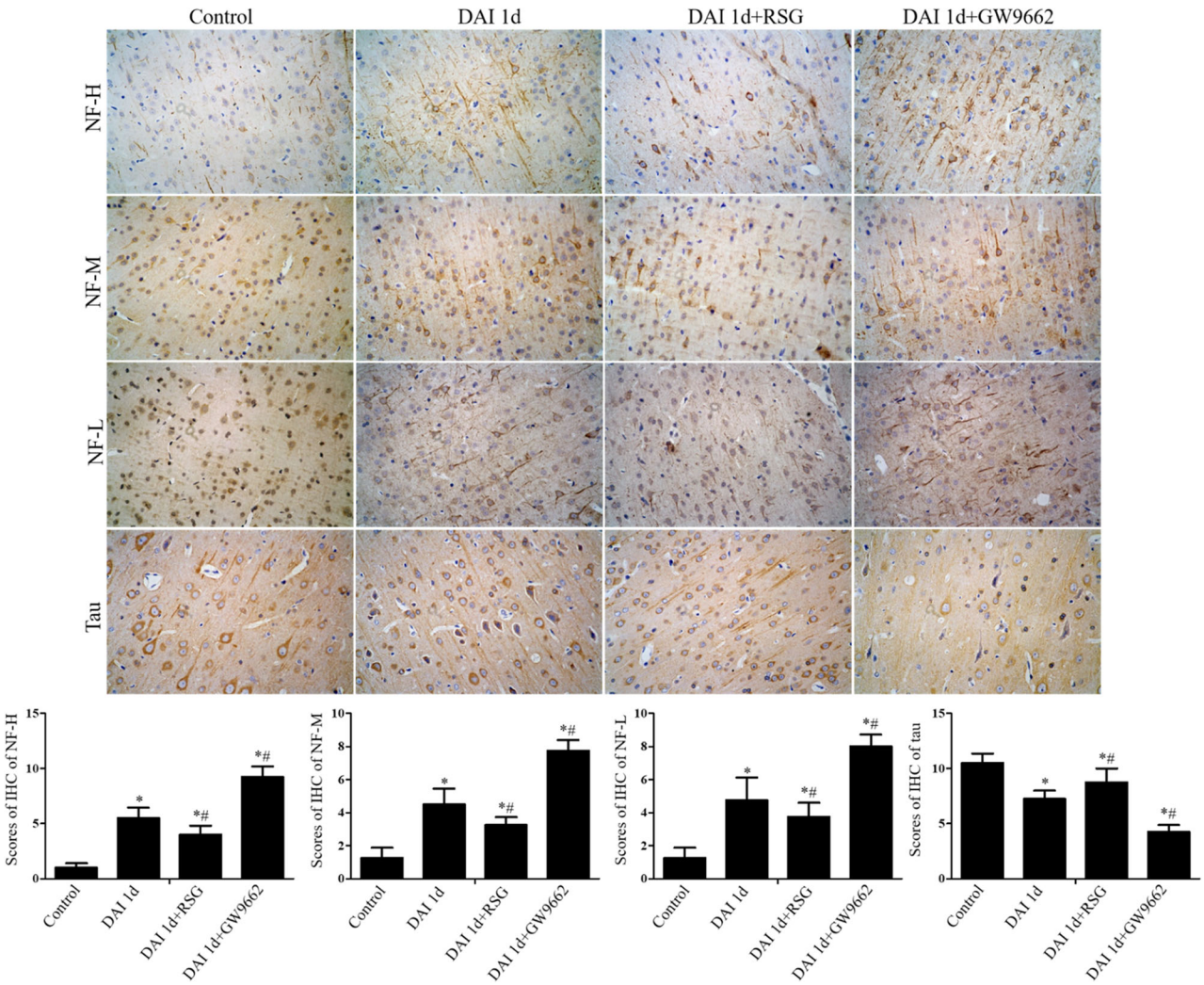

Fig. 2. Effects of PPARγ agonists and antagonists on the expression levels of axonal injury markers (NF-L, NF-M, NF-H, and tau) assessed by immunohistochemical staining (× 40 magnification, $n = 6$). The bar graphs show the statistical analysis of the levels of expression of NF-L, NF-M, NF-H, and tau (*$P < 0.05$, compared with the control group; $^{\#}P < 0.05$, compared with the DAI 1 d group). The relative expression of all proteins was assessed by IHS. Data are presented as the mean ± SD from three separate experiments.

increased after DAI. Importantly, treatment with RSG clearly decreased the Evans blue content, reflecting an improved integrity of the BBB, whereas the GW9662 antagonist had the opposite effect (Fig. 5). In normal rat brain, the structures surrounding the microvessels were intact, without interstices, edema, or distortion. In contrast, the structures surrounding the microvessels were injured following DAI, with large interstices and edema (Fig. 5). In agreement with the Evans blue results, RSG mitigated the tissue damage, whereas the GW9662 antagonist aggravated it, with tissues showing more interstices and edema.

Effects of the PPARγ Agonist and Antagonist on the Expression of TJ Proteins, Caveolin-1, and Inflammatory Factors

Western blot analysis was performed to examine the expression of BBB TJ proteins, such as occluding-1, ZO-1, and claudin-5, after DAI. The results showed that the levels of expression of TJ proteins decreased following DAI, indicating that the BBB was disrupted. RSG treatment resulted in significantly higher levels of expression of occluding-1, ZO-1, and claudin-5 in the rat cortex when compared with the DAI 1 d group, whereas GW9662 had

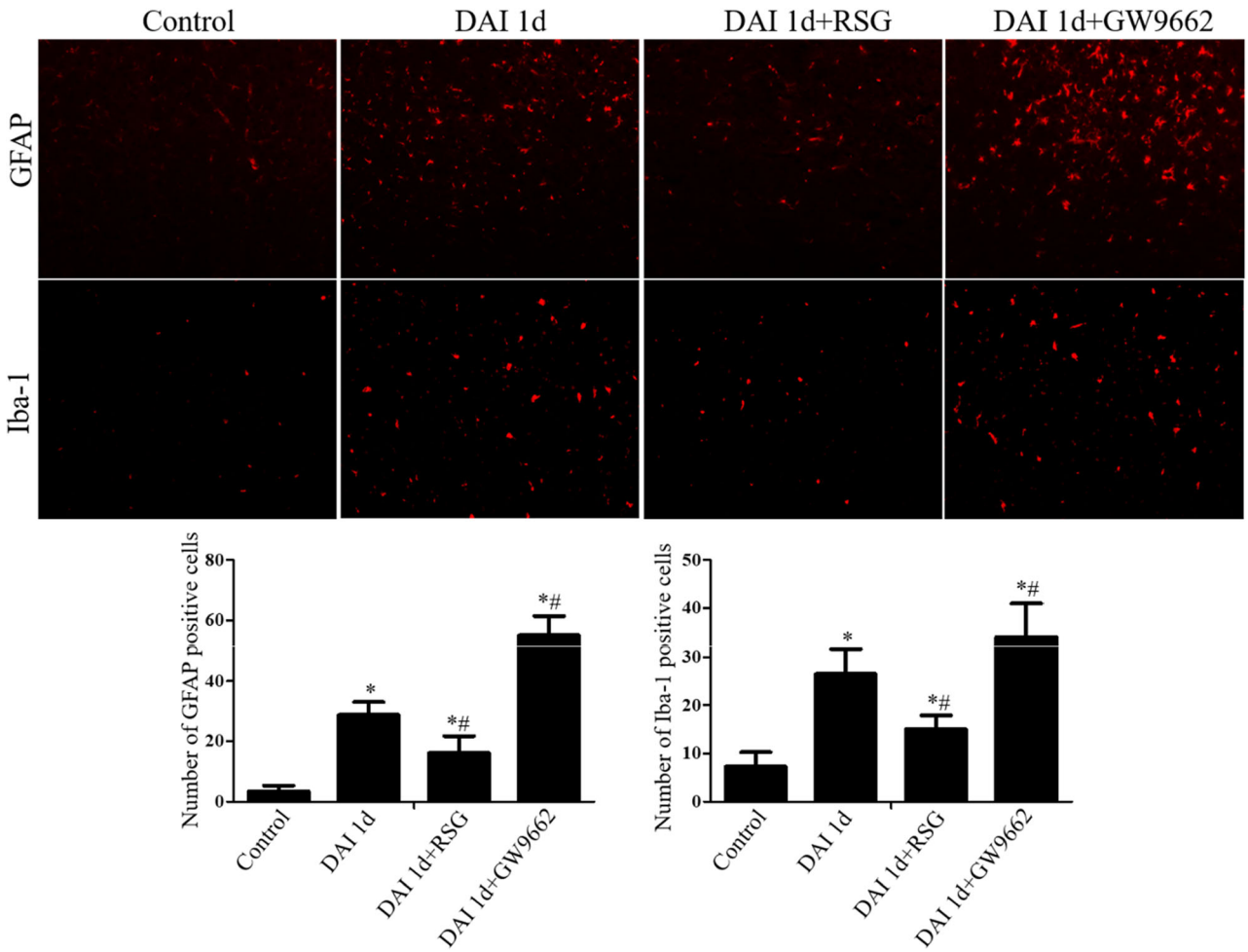

Fig. 3. Effects of PPARγ agonists and antagonists on the expression levels of glial response markers (Iba-1 and GFAP) assessed by immunofluorescence staining (× 40 magnification, $n = 6$). The bar graphs show the statistical analysis of the number of Iba-1 and GFAP-positive cells in the different experimental groups (*$P < 0.05$, compared with the control group; #$P < 0.05$, compared with the DAI 1 d group). Data are presented as the mean ± SD from three separate experiments.

the opposite effect. The expression of caveolin-1 was slightly higher after DAI, and RSG strongly enhanced this expression, while GW9662 treatment had the opposite effect (Fig. 6). In addition, the levels of expression of inflammatory mediators, including TNF-α, IL-1β, and IL-6, were determined by ELISA (Fig. 6). The levels of expression of these inflammation mediators increased after DAI. When compared with the DAI 1 d group, the levels of these inflammatory mediators decreased in the DAI 1 d + RSG group, but increased in the DAI 1 d + GW9662 group.

Localization of Caveolin-1 in the CNS Following DAI

To investigate the distribution of caveolin-1 in the rat cortex 1 day after DAI, tissues were double-stained with caveolin-1-specific and cell-specific antibodies and examined by immunofluorescence. The cell-specific antibodies recognized NeuN (a neuron-specific marker), GFAP (an astrocyte-specific marker), Iba-1 (a microglia-specific marker), and CD34 (an endothelium-specific marker). The results showed that caveolin-1 was predominantly expressed in vascular endothelial cells after DAI (Fig. 7).

RSG Protects the BBB Through a Caveolin-1-Dependent Pathway *in vitro*

To investigate the possible role played by caveolin-1 in the previously described effects of RSG, we downregulated its expression *in vitro* with siRNA. To determine the feasibility and efficiency of siRNA transfection, the cell monolayer (BBB model) was treated with caveolin-1

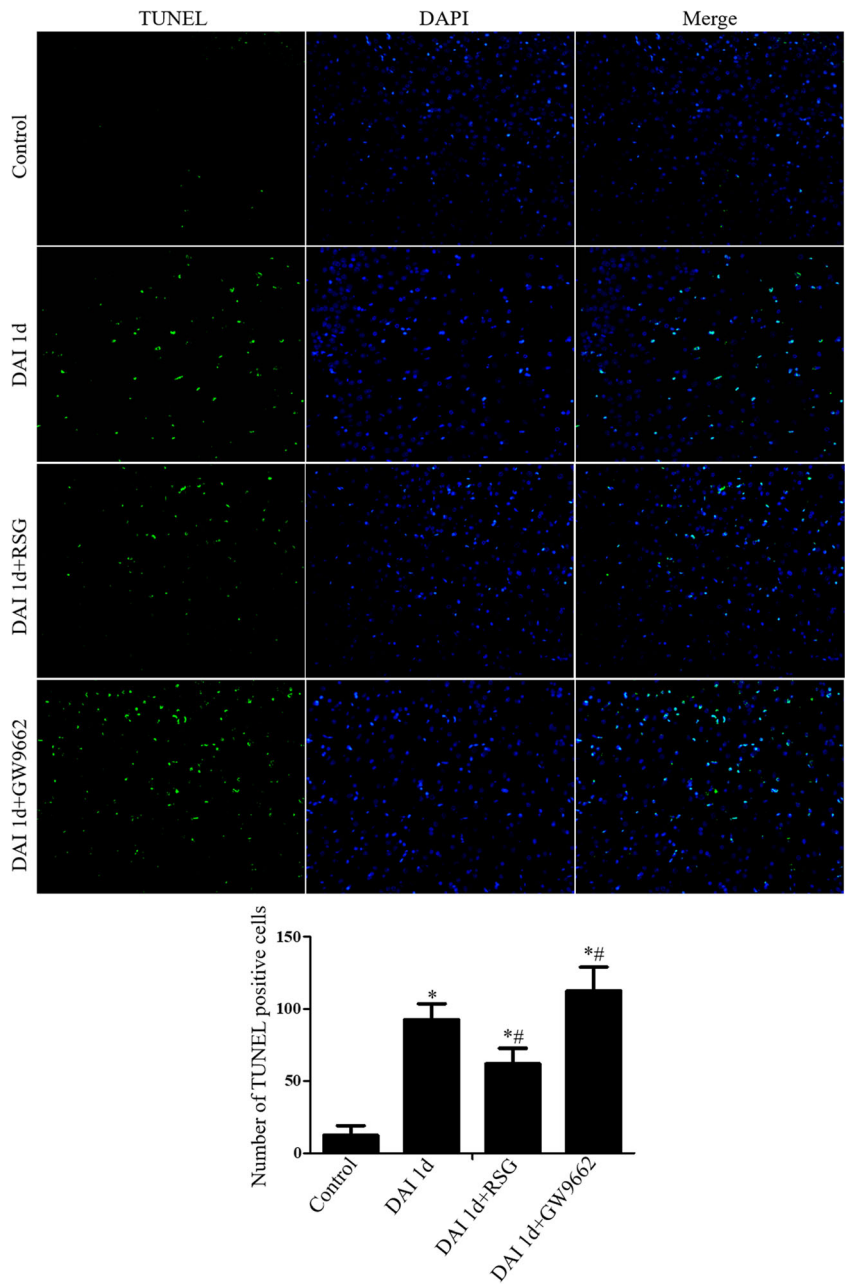

Fig. 4. Effects of PPARγ agonists and antagonists on cellular apoptosis, assessed by TUNEL (× 40 magnification, $n = 6$). The bar graphs show the statistical analysis of the number of TUNEL-positive cells in the different experimental groups (*$P < 0.05$, compared with the control group; $^{\#}P < 0.05$, compared with the DAI 1 d group). Data are presented as the mean ± SD from three separate experiments.

siRNA and analyzed by Western blot. The results showed that the expression levels of caveolin-1 did not differ between the control group and the control siRNA group. In contrast, caveolin-1 siRNA reduced the levels of expression of caveolin-1 24 h after transfection (Fig. 8).

The TEER and HRP flux were measured to assess the integrity of the *in vitro* BBB model in response to different stimuli and treatments. Compared to control group, the TEER decreased, whereas the HRP flux increased in OGD group. RSG treatment significantly increased TEER and decreased

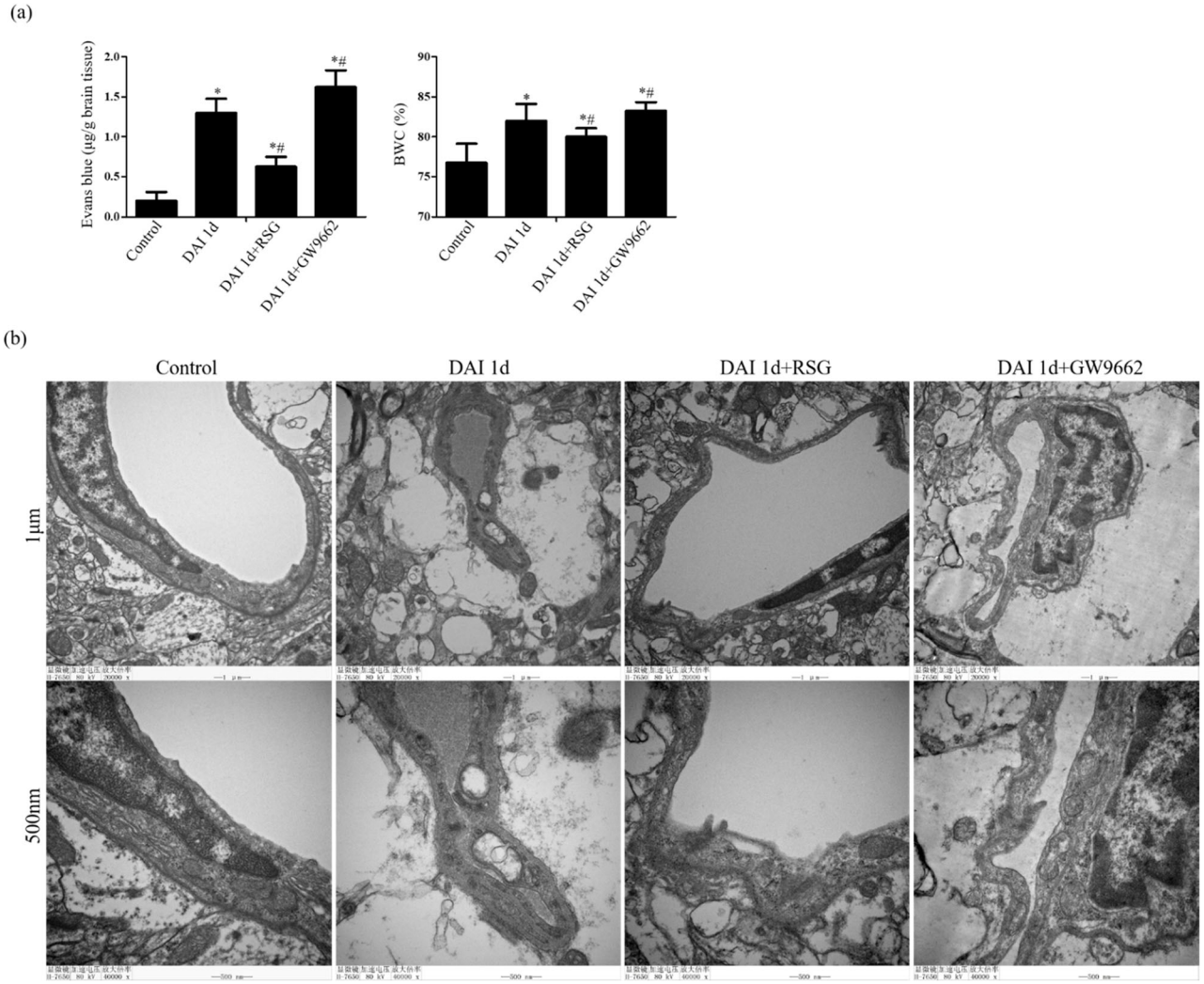

Fig. 5. Effects of PPARγ agonists and antagonists on the permeability and integrity of the BBB following DAI. **a** The bar graphs show the statistical analysis of the Evans blue diffusion and BWC values ($^{*}P < 0.05$, compared with the control group; $^{\#}P < 0.05$, compared with the DAI 1 d group). Data are presented as the mean ± SD from three separate experiments. **b** Ultrastructural alterations surrounding the microvessels after DAI and effects of the PPARγ agonist and antagonist, observed by TEM examination (× 40,000 magnification, $n = 6$).

the HRP flux. However, compared to OGD + RSG group, the protective effect of RSG was abrogated in the OGD + cav-1 siRNA + RSG group, indicating that RSG protects the BBB through a caveolin-1-dependent pathway *in vitro* (Fig. 8).

In vitro, RSG Increased the Expression of TJ Proteins and Decreased the Level of Inflammatory Cytokines Through a Caveolin-1-Dependent Pathway

Western blots were performed to assess the expression of TJ proteins and ELISAs were carried out to examine the levels of inflammatory cytokines. The results showed that after OGD, the expression of occluding-1, ZO-1, and claudin-5 decreased, while the levels of TNF-α, IL-1β, and IL-6 increased with respect to the control group (Fig. 9). However, RSG treatment significantly increased the expression of occluding-1, ZO-1, and claudin-5 and decreased the levels of TNF-α, IL-1β, and IL-6 when compared with the OGD group. All these protective effects of RSG were abrogated if caveolin-1 was downregulated, as seen in the OGD + cav-1 siRNA+RSG group (Fig. 9). These results indicate that RSG protected the BBB model

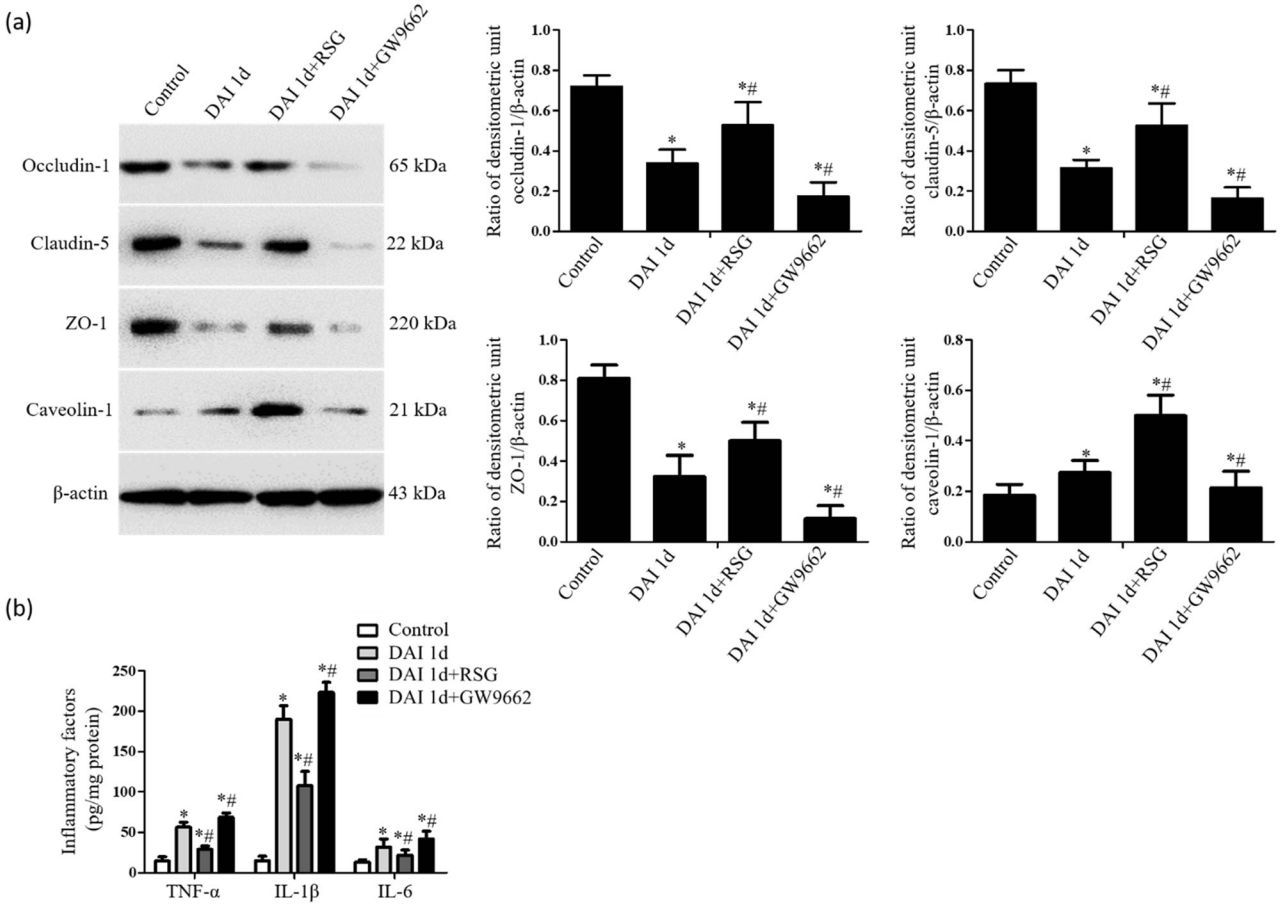

Fig. 6. Effects of the PPARγ agonist and antagonist on the levels of expression of TJ proteins, caveolin-1, and inflammatory mediators. **a** The expression levels of TJ proteins, including occluding-1, ZO-1, and claudin-5, as well as of caveolin-1 in the cortex were determined by Western blot. β-actin was used as an internal control. The bar graphs show the statistical analysis of the expression levels of occluding-1, ZO-1, claudin-5, and caveolin-1 in the different experimental groups. **b** The effects of the PPARγ agonist and antagonist on the levels of expression of inflammatory mediators, including TNF-α, IL-1β, and IL-6, in the rat cortex following DAI were determined by ELISA. All data are presented as the mean ± SD from three separate experiments ($n = 6$; $^{*}P < 0.05$, compared with the control group; $^{\#}P < 0.05$, compared with the DAI 1 d group).

in vitro by increasing the expression of TJ proteins and decreasing the levels of expression of inflammatory cytokines through a caveolin-1-dependent pathway.

DISCUSSION

The underlying mechanisms that explain how RSG protects the BBB from injury after DAI are still not completely understood. In this study, we discovered that PPARγ activation by RSG reduced cell apoptosis, the glial response, and axonal damage in a rat model of DAI. This protective effect correlated with increased expression of TJ proteins and reduced production of proinflammatory cytokines, such as IL-6, IL-1β, and TNF-α, *in vivo*. In contrast, PPARγ inhibition exacerbated tissue damage after DAI. Caveolin-1 was found to localize mainly in vascular endothelial cells in the rat cortex. Further experiments with HBMEC monolayers subjected to OGD showed that the protective effects of RSG on BBB integrity depended on caveolin-1.

DAI is considered as one of the most common and important pathological mechanisms triggered by TBI. The emerging therapeutic direction targets on specific pathophysiological changes including cytoskeleton stabilization, ion homeostasis, and protease inhibition. Although each of these approaches results in various degrees of axonal protection, more investigation is needed.

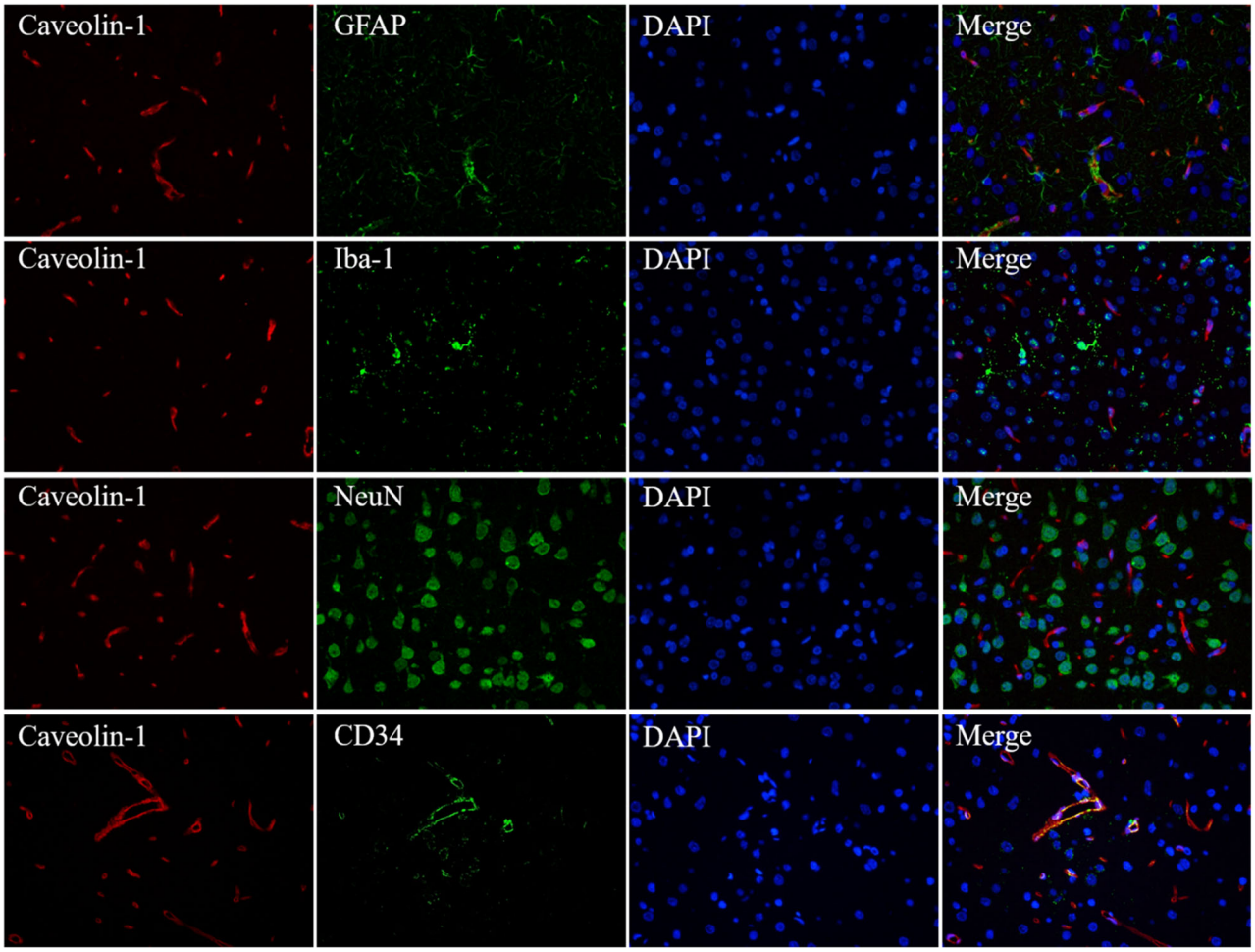

Fig. 7. Localization of caveolin in the rat cortex 1 day after DAI. Double immunofluorescence staining was performed with an antibody specific for caveolin-1 (red) and with antibodies that recognize either NeuN (a marker for neurons, green), GFAP (a marker for astrocytes, green), Iba-1 (a marker for microglia, green), or CD34 (a marker for endothelium) (× 40 magnification, $n = 6$).

The PPARγ is a member of the nuclear receptor superfamily and drugs that modulate its activity are used as insulin sensitizers for the treatment of type 2 diabetes mellitus. This receptor may regulate gene expression through various ligand-dependent and independent molecular processes. Previous studies have shown that PPARγ agonists exhibit a neuroprotective role by attenuating mitochondrial dysfunction, microglial activation, cognitive impairment, cortical tissue loss, and inflammation, and by suppressing neuronal autophagy and apoptosis following traumatic brain injury [23]. Here, a PPARγ agonist was found to protect from axonal injury, in agreement with our previous and other studies. In this study, we further confirmed that PPARγ activation or inhibition influenced cell apoptosis, the glial response, and axonal damage in a rat DAI model, supporting the notion that it plays a neuroprotective role after DAI.

Although the BBB protects the CNS from the immune system response, it becomes more permeable during inflammation. In this study, RSG reduced brain edema and attenuated the damage to the BBB induced by DAI, as shown by the decreased production of proinflammatory mediators like TNF-α, IL-1β, and IL-6. In this regard, it has been reported that the PPARγ agonist pioglitazone can also decrease the production of proinflammatory mediators like iNOS, TNF-α, and IL-1β [24]. Proinflammatory mediators are closely linked to the regulation of BBB permeability [25]. For example,

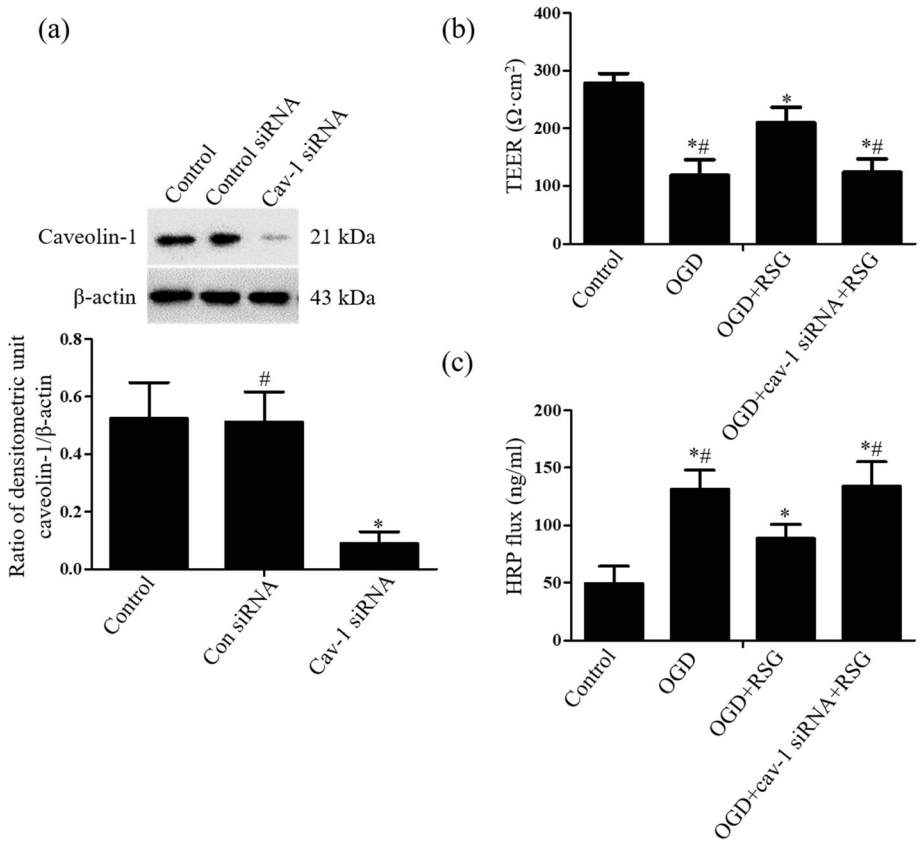

Fig. 8. *In vitro*, RSG protected the BBB through a caveolin-1-dependent pathway. **a** The expression of caveolin-1 in caveolin-1 siRNA- or control siRNA-treated cells was assessed by Western blot. β-actin expression was used as an internal control. Values represent the mean ± SD ($n = 6$; $^{\#}P > 0.05$, compared with the control group; compared with the control siRNA group, $^{*}P < 0.05$). **b**, **c** TEER and HRP flux were measured to assess the integrity of the BBB *in vitro*. All data are presented as the mean ± SD from three separate experiments ($n = 6$; $^{*}P < 0.05$, compared with the control group; $^{\#}P < 0.05$, compared with the OGD + RSG group).

TNF-α increases the permeability of the blood–brain barrier to moderately sized molecules *via* a mechanism which appears to involve activation of soluble guanylate cyclase and a protein tyrosine kinase [26]. TNF-α can also downregulate the expression of the transmembrane tight junction strand protein occludin [27]. Systemic inflammation induced by IL-1β was shown to trigger sustained disruption of tight junction proteins [28]. A selective inhibitor of the IL-1β converting enzyme was shown to decrease the permeability of the BBB and to reduce brain edema by inhibiting JNK-mediated MMP-9 induction and the consequent preservation of the tight junction protein ZO-1 [29]. IL-6 levels are significantly higher after TBI and this has been associated with increased BBB permeability, suggesting that the increased IL-6 levels may disrupt the BBB [30–32].

Caveolin-1, an integral membrane protein located at caveolae in endothelial cells, plays an important role in many physiological and pathological BBB processes [7]. Caveolin-1 has been shown to prevent the degradation of TJ proteins and to protect BBB integrity by inhibiting RNS production and MMP activity [33]. In this study, caveolin-1 was found to be predominantly expressed in vascular endothelial cells after DAI. PPARγ has also been detected in human vascular endothelial cells [34].

It is worth mentioning that the effects of PPARγ activation on the expression of caveolin-1 seem to differ in different cell types. RSG was shown to upregulate caveolin-1 expression in THP-1 cells through a PPAR-dependent mechanism [9]. In our study, we found that PPARγ activation by RSG also increased the expression of caveolin-1, both *in vivo* and *in vitro*. Previous studies

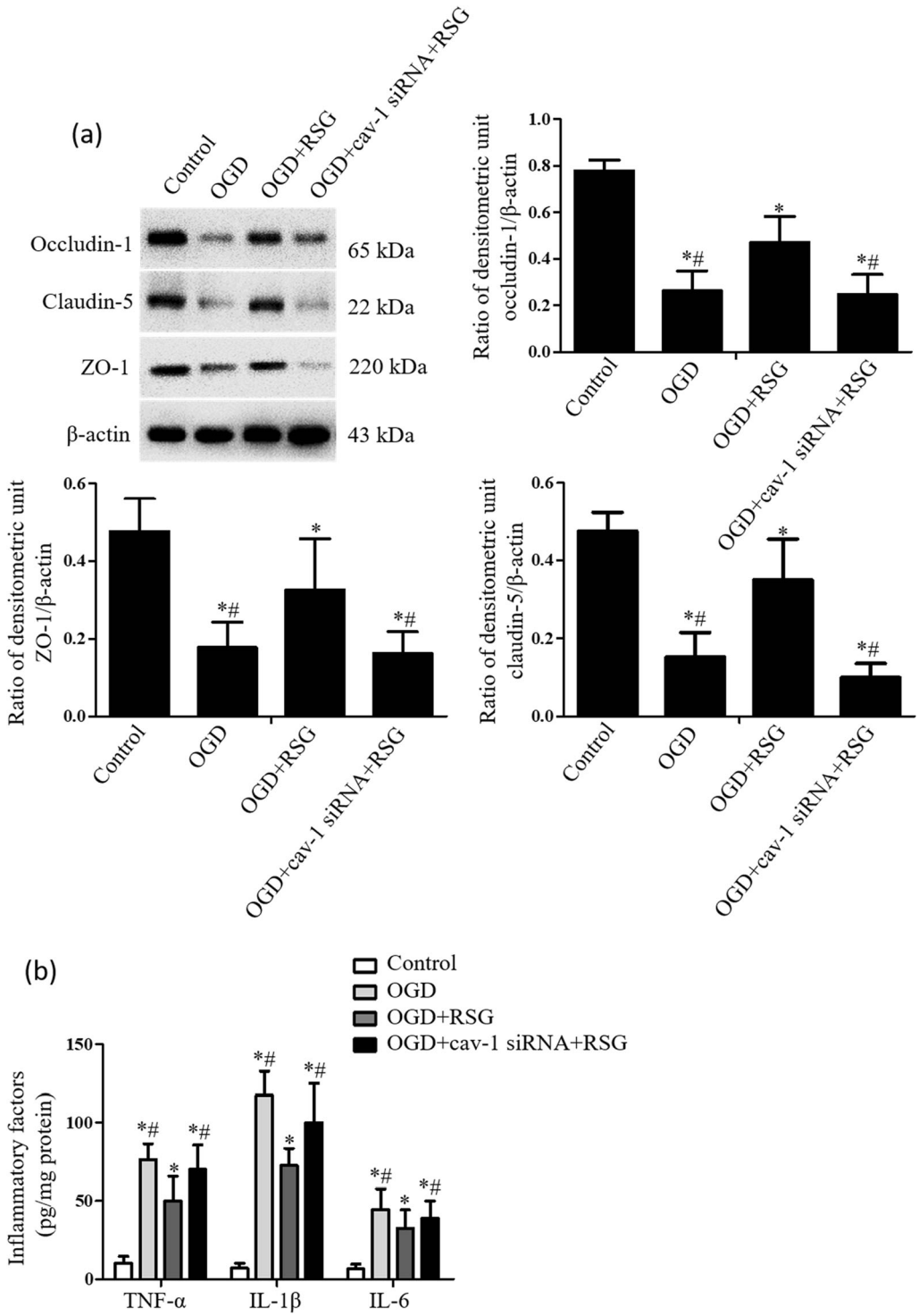

Fig. 9. *In vitro*, RSG increased the expression of TJ proteins and decreased the levels of inflammatory cytokines through a caveolin-1-dependent pathway. **a** Expression of occluding-1, ZO-1, and claudin-5, assessed by Western blot. The expression of β-actin was used as an internal control. The bar graphs show the statistical analysis of the levels of expression of occluding-1, ZO-1, and claudin-5. **b** The levels of expression of inflammatory mediators, including TNF-α, IL-1β, and IL-6 in each group were determined by ELISA. Data represent the mean ± SD from three separate experiments ($n = 6$; $^{*}P < 0.05$, compared with the control group; $^{\#}P < 0.05$, compared with the OGD + RSG group).

showed that PPARγ upregulated caveolin-1 expression in human carcinoma cells [35], and PPARγ gene therapy induced caveolin-1 expression and enhanced cholesterol efflux in apoE-deficient mice [36]. PPARγ has also been shown to play a central role in normal thyroid physiology by upregulating caveolin-1 [37]. However, PPARγ activation inhibited caveolin-1 protein expression by promoting its lysosomal degradation in rat distal pulmonary arterial smooth muscle cells under hypoxia [38]. By means of an *in vitro* BBB model subjected to OGD, we found that RSG protected the integrity of the BBB through a caveolin-1-dependent pathway. After downregulating the expression of caveolin-1 with siRNA, the neuroprotective effect of RSG following OGD was abrogated.

In conclusion, our findings indicate that PPARγ activation reduces axonal injury, cell apoptosis, and glia activation and maintains BBB integrity by upregulating the expression of TJ proteins and inhibiting the release of inflammatory mediators, accompanied by increased expression of caveolin-1. The protective effect of RSG seen in the *in vitro* BBB model after OGD was abrogated by silencing of caveolin-1 mRNA. Our results indicate that the PPARγ agonist RSG can protect BBB integrity by decreasing the levels of inflammatory mediators through a caveolin-1-dependent pathway.

AUTHOR CONTRIBUTIONS

Yonglin Zhao designed the concept of the work and the experiments, did the experiments, and wrote the manuscript. Jin Qin and Jinning Song contributed to the initial idea and conceived the study design. Ming Zhang and Tingqin Huang helped draft and revise the manuscript. Xing Wei performed the analyses and designed the figures. All authors approved the manuscript.

FUNDING INFORMATION

This work was financially supported by the Natural Science Foundation of Shaanxi Province (Grant No. 2018JQ8063) to Jie Qin.

COMPLIANCE WITH ETHICAL STANDARDS

All procedures were performed according to the Guidelines and Suggestions for the Care and Use of Laboratory Animals formulated by the Ministry of Science and Technology of the People's Republic of China (PRC) and the Guidelines for the Care and Use of Laboratory Animals from the National Institutes of Health (NIH Publication no. 80-23). The Biomedical Ethics Committee for Animal Experiments of Shaanxi Province (China) approved this study.

Conflict of Interest. The authors declare that there is no personal or institutional conflict of interest related to the presented research and its publication.

REFERENCES

1. Blanchette, M., and R. Daneman. 2015. Formation and maintenance of the BBB. *Mechanisms of Development* 138 (Pt 1): 8–16.
2. Coisne, C., and B. Engelhardt. 2011. Tight junctions in brain barriers during central nervous system inflammation. *Antioxidants & Redox Signaling* 15 (5): 1285–1303.
3. Fakhoury, M. 2015. Role of immunity and inflammation in the pathophysiology of neurodegenerative diseases. *Neurodegenerative Diseases* 15 (2): 63–69.
4. Liu, H., M.E. Rose, S. Culver, X. Ma, C.E. Dixon, and S.H. Graham. 2016. Rosiglitazone attenuates inflammation and CA3 neuronal loss following traumatic brain injury in rats. *Biochemical and Biophysical Research Communications* 472 (4): 648–655.
5. Yao, J., K. Zheng, and X. Zhang. 2015. Rosiglitazone exerts neuroprotective effects via the suppression of neuronal autophagy and apoptosis in the cortex following traumatic brain injury. *Molecular Medicine Reports* 12 (5): 6591–6597.
6. Zhao, Yong-Lin, Jin-Ning Song, et al. 2016. Rosiglitazone ameliorates diffuse axonal injury by reducing loss of tau and up-regulating caveolin-1 expression. *Neural Regeneration Research* 11 (6): 944–950.
7. Zhao, Y.L., J.N. Song, and M. Zhang. 2014. Role of caveolin-1 in the biology of the blood-brain barrier. *Reviews in the Neurosciences* 25 (2): 247–254.
8. Mandrekar-Colucci, S., A. Sauerbeck, P.G. Popovich, and D. McTigue. 2013. PPAR agonists as therapeutics for CNS trauma and neurological diseases. *ASN Neuro* 5 (5): e00129–e00129.
9. Llaverias, G., M. Vázquez-Carrera, R.M. Sánchez, et al. 2004. Rosiglitazone upregulates caveolin-1 expression in THP-1 cells through a PPAR-dependent mechanism. *Journal of Lipid Research* 45 (11): 2015–2024.
10. Zhao, Y., J. Zhao, M. Zhang, et al. 2017. Involvement of toll like receptor 2 signaling in secondary injury during experimental diffuse axonal injury in rats. *Mediators of Inflammation* 1570917: 2017.
11. Ramirez, S.H., D. Heilman, B. Morsey, R. Potula, J. Haorah, and Y. Persidsky. 2008. Activation of peroxisome proliferator-activated receptor gamma (PPARγ) suppresses Rho GTPases in human brain microvascular endothelial cells and inhibits adhesion and transendothelial migration of HIV-1 infected monocytes. *Journal of Immunology* 180 (3): 1854–1865.
12. Lombardi, A., G. Cantini, E. Piscitelli, S. Gelmini, M. Francalanci, T. Mello, E. Ceni, G. Varano, G. Forti, M. Rotondi, A. Galli, M. Serio, and M. Luconi. 2008. A new mechanism involving ERK contributes to rosiglitazone inhibition of tumor necrosis factor-alpha and interferon-gamma inflammatory effects in human

endothelial cells. *Arteriosclerosis, Thrombosis, and Vascular Biology* 28 (4): 718–724.
13. Jin, X., Y. Sun, J. Xu, and W. Liu. 2015. Caveolin-1 mediates tissue plasminogen activator-induced MMP-9 upregulation in cultured brain microvascular endothelial cells. *Journal of Neurochemistry* 132 (6): 724–730.
14. Gu, Y., G. Zheng, M. Xu, Y. Li, X. Chen, W. Zhu, Y. Tong, S.K. Chung, K.J. Liu, and J. Shen. 2012. Caveolin-1 regulates nitric oxide-mediated matrix metalloproteinases activity and blood-brain barrier permeability in focal cerebral ischemia and reperfusion injury. *Journal of Neurochemistry* 120 (1): 147–156.
15. Ye, L.B., X.C. Yu, Q.H. Xia, Y. Yang, D.Q. Chen, F. Wu, X.J. Wei, X. Zhang, B.B. Zheng, X.B. Fu, H.Z. Xu, X.K. Li, J. Xiao, and H.Y. Zhang. 2016. Regulation of caveolin-1 and junction proteins by bFGF contributes to the integrity of blood-spinal cord barrier and functional recovery. *Neurotherapeutics* 13 (4): 844–858.
16. Long, M., S.H. Huang, C.H. Wu, G.M. Shackleford, and A. Jong. 2012. Lipid raft/caveolae signaling is required for Cryptococcus neoformans invasion into human brain microvascular endothelial cells. *Journal of Biomedical Science* 19: 19.
17. Dong, H.J., C.Z. Shang, D.W. Peng, J. Xu, P.X. Xu, L. Zhan, and P. Wang. 2014. Curcumin attenuates ischemia-like injury induced IL-1beta elevation in brain microvascular endothelial cells via inhibiting MAPK pathways and nuclear factor-kappaB activation. *Neurological Sciences* 35 (9): 1387–1392.
18. Yang, F., S. Liu, C. Yu, S.J. Wang, A. Paganini-Hill, and M.J. Fisher. 2012. PDE4 regulates tissue plasminogen activator expression of human brain microvascular endothelial cells. *Thrombosis Research* 129 (6): 750–753.
19. Miao, Z., Y. Dong, W. Fang, D. Shang, D. Liu, K. Zhang, B. Li, and Y.H. Chen. 2014. VEGF increases paracellular permeability in brain endothelial cells via upregulation of EphA2. *The Anatomical Record (Hoboken)* 297 (5): 964–972.
20. Zhou, J.X., G.R. Ding, J. Zhang, Y.C. Zhou, Y.J. Zhang, and G.Z. Guo. 2013. Detrimental effect of electromagnetic pulse exposure on permeability of in vitro blood-brain-barrier model. *Biomedical and Environmental Sciences* 26 (2): 128–137.
21. Lin, M.N., D.S. Shang, W. Sun, B. Li, X. Xu, W.G. Fang, W.D. Zhao, L. Cao, and Y.H. Chen. 2013. Involvement of PI3K and ROCK signaling pathways in migration of bone marrow-derived mesenchymal stem cells through human brain microvascular endothelial cell monolayers. *Brain Research* 1513: 1–8.
22. Soslow, R.A., A.J. Dannenberg, D. Rush, et al. 2015. COX-2 is expressed in human pulmonary, colonic, and mammary tumors. *Cancer* 89 (12): 2637–2645.
23. Liu, M., A.D. Bachstetter, W.A. Cass, J. Lifshitz, and G. Bing. 2017. Pioglitazone attenuates Neuroinflammation and promotes dopaminergic neuronal survival in the nigrostriatal system of rats after diffuse brain injury. *Journal of Neurotrauma* 34 (2): 414–422.
24. Sauerbeck, A., J. Gao, R. Readnower, M. Liu, J.R. Pauly, G. Bing, and P.G. Sullivan. 2011. Pioglitazone attenuates mitochondrial dysfunction, cognitive impairment, cortical tissue loss, and inflammation following traumatic brain injury. *Experimental Neurology* 227 (1): 128–135.
25. Cunningham, T.L., Cartagena, C.M., Lu, X.-C., et al. 2013. Correlations between blood-brain barrier disruption and neuroinflammation in an experimental model of penetrating ballistic-like brain injury.
26. Mayhan, W.G. 2002. Cellular mechanisms by which tumor necrosis factor-alpha produces disruption of the blood-brain barrier. *Brain Research* 927 (2): 144–152.
27. Mankertz, J., S. Tavalali, H. Schmitz, et al. 2000. Expression from the human occludin promoter is affected by tumor necrosis factor alpha and interferon gamma. *Journal of Cell Science* 113 (Pt 11): 2085–2090.
28. McColl, B.W., N.J. Rothwell, and S.M. Allan. 2008. Systemic inflammation alters the kinetics of cerebrovascular tight junction disruption after experimental stroke in mice. *The Journal of Neuroscience* 28 (38): 9451–9462.
29. Sozen, T., R. Tsuchiyama, Y. Hasegawa, H. Suzuki, V. Jadhav, S. Nishizawa, and J.H. Zhang. 2009. Role of interleukin-1beta in early brain injury after subarachnoid hemorrhage in mice. *Stroke* 40 (7): 2519–2525.
30. Uchida, T., M. Mori, A. Uzawa, H. Masuda, M. Muto, R. Ohtani, and S. Kuwabara. 2017. Increased cerebrospinal fluid metalloproteinase-2 and interleukin-6 are associated with albumin quotient in neuromyelitis optica: Their possible role on blood-brain barrier disruption. *Multiple Sclerosis* 23 (8): 1072–1084.
31. Takeda, S., N. Sato, K. Ikimura, H. Nishino, H. Rakugi, and R. Morishita. 2013. Increased blood-brain barrier vulnerability to systemic inflammation in an Alzheimer disease mouse model. *Neurobiology of Aging* 34 (8): 2064–2070.
32. Farbood, Y., A. Sarkaki, M. Dianat, A. Khodadadi, M.K. Haddad, and S. Mashhadizadeh. 2015. Ellagic acid prevents cognitive and hippocampal long-term potentiation deficits and brain inflammation in rat with traumatic brain injury. *Life Sciences* 124: 120–127.
33. Gu, Y., C.M. Dee, and J. Shen. 2011. Interaction of free radicals, matrix metalloproteinases and caveolin-1 impacts blood-brain barrier permeability. *Frontiers in Bioscience (Scholar Edition)* 3: 1216–1231.
34. Delerive, P., F. Martin-Nizard, G. Chinetti, et al. 1999. Peroxisome proliferator-activated receptor activators inhibit thrombin-induced endothelin-1 production in human vascular endothelial cells by inhibiting the activator protein-1 signaling pathway. *Circulation Research* 85 (5): 394–402.
35. Burgermeister, E., L. Tencer, and M. Liscovitch. 2003. Peroxisome proliferator-activated receptor-gamma upregulates caveolin-1 and caveolin-2 expression in human carcinoma cells. *Oncogene* 22 (25): 3888–3900.
36. Hu, Q., X.J. Zhang, C.X. Liu, X.P. Wang, and Y. Zhang. 2010. PPARgamma1-induced caveolin-1 enhances cholesterol efflux and attenuates atherosclerosis in apolipoprotein E-deficient mice. *Journal of Vascular Research* 47 (1): 69–79.
37. Werion, A., V. Joris, M. Hepp, L. Papasokrati, L. Marique, C. de Ville de Goyet, V. van Regemorter, M. Mourad, B. Lengelé, C. Daumerie, E. Marbaix, S. Brichard, M.C. Many, and J. Craps. 2016. Pioglitazone, a PPARgamma agonist, upregulates the expression of caveolin-1 and catalase, essential for thyroid cell homeostasis: a clue to the pathogenesis of Hashimoto's thyroiditis. *Thyroid* 26 (9): 1320–1331.
38. Yang, K., W. Lu, Q. Jiang, X. Yun, M. Zhao, H. Jiang, and J. Wang. 2015. Peroxisome proliferator-activated receptor gamma-mediated inhibition on hypoxia-triggered store-operated calcium entry. A caveolin-1-dependent mechanism. *American Journal of Respiratory Cell and Molecular Biology* 53 (6): 882–892.